Properties of Pt-supported Co nanomagnets from relativistic density functional theory calculations

Adriano Mosca Conte,* Stefano Fabris, and Stefano Baroni
SISSA—Scuola Internazionale Superiore di Studi Avanzati, via Beirut 2-4, I-34014 Trieste, Italy, and INFM-CNR DEMOCRITOS, Theory@Elettra group, corner of Sincrotrone Trieste, Area Science Park, I-34012 Basovizza, Trieste, Italy
(Received 16 April 2008; published 11 July 2008)

The electronic, structural, and magnetic properties of Co-based low-dimensional nanostructures supported by Pt surfaces are investigated using computer simulations based on density functional theory. The effects of the local orientation of the magnetization, including the magnetic anisotropy energy, are accounted for within a noncollinear spin-density functional theory formalism where the spin-orbit interaction is described by fully relativistic ultrasoft pseudopotentials. The magnetic moments, the direction of the easy-magnetization axis, and the anisotropy energy are compared with available experimental and theoretical data, and are shown to be extremely sensitive to the local atomic environment of the Co adatoms. We argue that this sensitivity could be exploited to tailor the properties of magnetic devices by engineering the local environment and/or the operating conditions of nanomagnets.

DOI: 10.1103/PhysRevB.78.014416 PACS number(s): 75.75.+a, 71.15.Mb, 73.22.−f

I. INTRODUCTION

Molecular nanomagnets are gaining an ever increasing importance in science and technology for their potential applications in such diverse fields as electronics,[1,2] catalysis,[3] and biochemistry.[4] This interest stems from their behavior as single-domain magnets, whose dimensions can be scaled down from the micrometer to the nanometer scale.[5–8] In the case of electronic applications for instance, one of the main challenges is to reduce the size of magnetic storage media, preventing at the same time the mutual interaction between individual memory units.[9] Single-domain magnetic nanoparticles supported by nonmagnetic surfaces are among the most promising systems for this purpose, and have been the subject of intense experimental and theoretical work.[10–14]

While the magnetic properties of bulk systems (at least those where strong correlations do not play a significant role) are well understood, the mechanisms controlling the magnetic properties of nanomagnets are not yet clear at the same level of detail. In principle, nanowires [one dimensional (1D)] and single-domain (0D) nanoparticles cannot form stable magnetically ordered structures at any finite temperature.[15,16] However, below the so-called blocking temperature, these systems may be able to maintain a ferromagnetic order for a period that can be much longer than the typical experimental observation time or the operation time of a device. Magnetism in low-dimensional systems is therefore a kinetic effect due to the stabilizing action of the magnetic anisotropy resulting from the spin-orbit interaction. It is this phenomenon that allows for magnetism in low-dimensional systems such as the Co nanowire supported by a (997)-Pt surface[17] or the Co adatom on Pt surface,[10] which are the subject of this study. The ferromagnetic behavior of these low-dimensional systems has been confirmed by the presence of a magnetic hysteresis loop below the blocking temperature,[18] and can be traced back to the magnetic anisotropy of materials, which is ultimately due to relativistic spin-orbit effects.

In this paper we use density functional theory (DFT) to investigate the structural, electronic, and magnetic properties of low-dimensional systems and nanostructures. In particular, we focus on the magnetic anisotropy energy (MAE) that controls the observable magnetism in these systems below the blocking temperature. Spin-orbit effects are usually included in all-electron DFT calculations often in conjunction with some shape approximation on the potential, such as, for example, the Korringa-Kohn-Rostoker (KKR) method[19,20] or the linear muffin-tin orbital method with the atomic-sphere approximation (LMTO-ASA).[21] This is frequently done by either introducing a spin-orbit correction into an otherwise nonrelativistic or scalar-relativistic Hamiltonian, or by solving a fully relativistic Dirac-like Kohn-Sham (KS) equation. Due to their all-electron nature and to the shape approximations on the potentials, however, the ability of these implementations to efficiently and accurately predict the minimum-energy atomic geometry of the system is rather limited.

Plane-wave (PW) pseudopotential methods are instead perfectly suited to an efficient and accurate calculation of atomic forces, and, hence, to determine equilibrium geometries. Standard pseudopotentials, however, are usually limited to nonrelativistic calculations that cannot capture magnetic anisotropy effects. This is particularly so when ultrasoft pseudopotentials (USPPs) (Ref. 22) are used to describe the interaction of valence electrons with the core electrons of first-row transition-metal ions. Only recently has a fully relativistic USPP implementation been introduced and tested for bulk transition metals.[23] The method has been applied to predict colossal magnetoanisotropy in Pt nanowires.[24] In this work the fully relativistic USPP approach of Ref. 23 is used for a combined study of the atomistic and magnetic structures of Co adatoms and nanowires supported on Pt(111) and vicinal surfaces.

The paper is organized as follows: a theoretical framework is described in Sec. II. Our results on Co adatoms adsorbed on Pt(111) surfaces, and on Co nanowires supported by flat Pt(111) and stepped Pt(442) surfaces are presented and discussed in Sec. III. Concluding remarks are finally reported in Sec. IV.

II. THEORY FRAMEWORK

A. Calculating magnetic anisotropy energies

Within DFT, magnetic systems are most commonly studied using the collinear local spin-density approximation (LSDA) and neglecting spin-orbit effects. The calculation of the MAE and a detailed description of the magnetic structure, however, requires going beyond these approximations. One possibility to do so, which is popular in the literature, relies on the assumption that the self-consistent (SCF) charge density obtained at the LSDA level is not modified by changes in the magnetization direction when the spin-orbit interaction is included. Using this assumption and the so-called force theorem,[25] the MAE is often approximated from the SCF scalar-relativistic all-electron potential as the difference between the band energies (the sum of the occupied Kohn and Sham eigenvalues) calculated with and without account of the spin-orbit coupling. As a relevant example, this method is applied to a Co nanowire on a (664) Pt surface.[12] The band energy is computed for different directions of the magnetic moment of the Co atoms and the applicability of the force theorem is checked for a selected set of magnetic configurations by comparing the results with SCF calculations. An average deviation of 0.2 meV/atom between the two methods is estimated, corresponding to $\approx 10\%$ of the total MAE per unit cell. We stress that by its very nature, this approach neglects SCF (Hartree plus exchange and correlation) contributions to the MAE.

Here we use a different approach in which the MAE is calculated self-consistently on the basis of the total energy rather than in terms of the orbital eigenvalues only. Our method involves the introduction of one-particle bidimensional spinors as eigenstates of the KS equations.[26–28] The spin-orbit interaction is included in the nonlocal part of the fully relativistic pseudopotentials, as described in Refs. 26 and 23. No relativistic effects were taken into account in the parametrizations of the exchange and correlation functional.[29]

In principle, starting from a general initial direction of the magnetization, the minimization of the total energy would drive the system to the ground state, redirecting the magnetization along the easy axis. In practice, however, this is hampered by the very different energy scales, resulting from changing the absolute value of the individual magnetic moments ($\lesssim 10^{-1}$ eV) and the direction of the total magnetization ($\approx 10^{-3}$ eV). As a result, during the SCF procedure, the former converge much faster than the latter and a more efficient strategy has to be devised. To this end, instead of performing a unique and time-consuming SCF calculation, we perform a set of different SCF calculations, each corresponding to a different value of the initial direction of the total magnetization, which is constrained to its initial value during the SCF cycle. The method is then used to sample the MAE for the most relevant magnetization directions. This strategy allows us to identify the ground state, i.e., the magnetization direction with the lowest total energy, the energy landscape as a function of the magnetization direction, as well as the MAE obtained from the energy difference of the systems with the magnetization aligned along the easy and hard axes.

B. Calculation details

Our calculations are based on DFT within the LSDA for the exchange-correlation functional, using the PW pseudopotential method as implemented in the PWSCF code of the Quantum ESPRESSO distribution.[30] Atomic cores are represented by USPPs (Refs. 22 and 31); KS orbitals are expanded in PWs up to a kinetic-energy cutoff of 40 Ry, whereas PWs up to 400 Ry are used to represent the charge density. These energy cutoffs, unusually large for the USPP calculations, are necessary to accurately predict the small energy differences ($\approx$meV) arising from rotations of the magnetic moments. Atomic structures are optimized by using the Hellmann-Feynman forces and the scalar-relativistic pseudopotentials. At the end of the structural optimization, the force on each atom is smaller than 0.02 eV/Å. The fully relativistic pseudopotentials are employed for performing further structural relaxations in a few test cases. These calculations yield equilibrium atomic coordinates, which differ by less than 0.01 Å from those obtained with the scalar-relativistic pseudopotentials. The smallness of relativistic effects on the atomic geometry of the system does not come as a surprise. The strength of spin-orbit effects is of second order in the fine-structure constant ($\alpha = \frac{e^2}{\hbar c} \approx \frac{1}{137}$) and, while corrections to orbital energies are of first order in this strength, corrections to total energies are of second order, and hence of fourth order in α. Forces acting on atoms are derivatives of total energies so that relativistic corrections to atomic forces are also of order α^4, which are rather small indeed. This is in agreement with previous calculations[23] performed on Au-fcc and Pt-fcc bulk showing that the lattice constant has the same value if calculated with scalar or fully relativistic pseudopotentials (within an error of 0.01 a.u.).

Pt surfaces are modeled with the supercell slabs having the in-plane lattice parameter appropriate for bulk Pt-fcc (3.92 Å) and being separated by a vacuum region 10 Å thick. The Co adatom on the Pt (111) surface is modeled with a (4×4) 4-layer-thick supercell slab [Fig. 1(a)] so that the distance between the adatom and its nearest periodic images is 8.32 Å. The Co nanowire on the (111) surface is modeled by a (4×1) 4-layer-thick supercell [Fig. 1(b)] while vicinal surfaces are modeled as periodic arrays of *B*-type step edges separated by (111) terraces. The calculations are performed for such a (442) surface [Fig. 1(c)]. The small energy differences involved in the calculated MAE required the use of dense **k**-point meshes: The calculations for the Co nanowires and for the Co adatom have been performed by using the $(5\times15\times1)$ and $(5\times5\times1)$ Monkorst and Pack[32] **k**-point meshes. These meshes, together with a Methfessel-Paxton smearing parameter of 0.01 eV,[33] and the chosen basis set yield convergence in the total energy below 0.1 meV per cell.

The Co atoms (adatoms and nanowires) are positioned symmetrically on both sides of the supercell slabs (Fig. 1) with opposite initial magnetic moment, yielding zero total magnetization in all the calculations. We note that no differences in the structural and magnetic properties are observed in performing the same calculations while positioning the Co atoms on only one side of the supercell slab without mirror symmetry along the z axis.

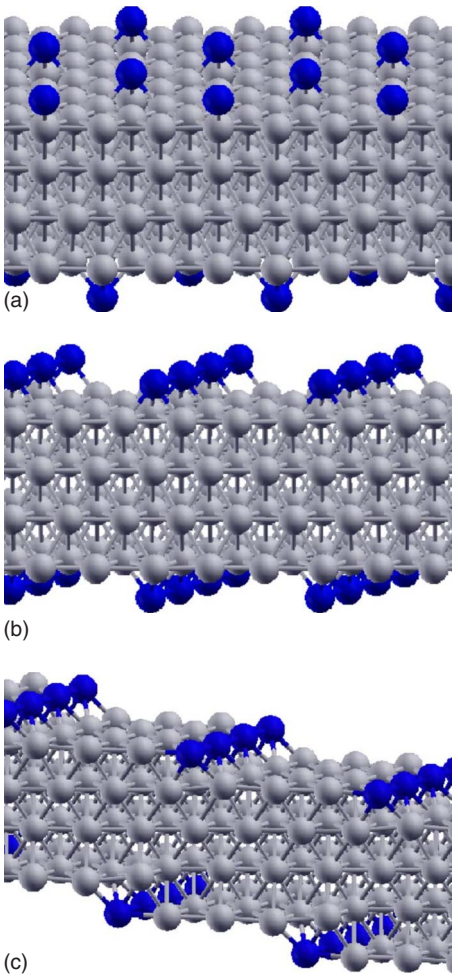

FIG. 1. (Color online) Super cells used to describe the Co nanostructures supported by Pt surfaces: (a) Co adatom on Pt(111), (b) Co nanowire on Pt(111), and (c) Co nanowire on Pt(442). Light gray spheres represent the surface Pt atoms while blue (dark gray) spheres represent the supported Co atoms.

With the purpose of comparing our results with the available literature, we consider, besides the fully relaxed geometries, also a set of reference geometries in which all the Pt-Pt and Co-Pt bond lengths have the equilibrium bulk value. Following the nomenclature employed in Refs. 12 and 13, we will refer to these configurations as *unrelaxed*.

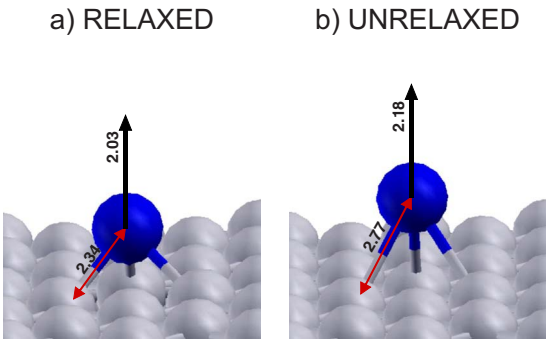

FIG. 2. (Color online) (a) Equilibrium and (b) unrelaxed adsorption geometries of a Co adatom on a Pt (111) surface. Red (gray) arrows indicate the Co-Pt bond lengths in angstrom while black arrows represent the magnetic moments directed along the easy-magnetization axis in units of μ_B. Atoms are represented as described in Fig. 1.

III. RESULTS AND DISCUSSION

A. Co adatom on the flat Pt(111) surface

We first address the case of a Co adatom adsorbed on the most stable fcc site of the Pt(111) surface. Adsorption on the hcp site is 0.1 eV higher in energy than on the fcc one. The equilibrium local environment and magnetic moments for the two sites are very similar with the difference in calculated quantities being always smaller than 2%. The side view of the equilibrium adsorption geometry is shown in Fig. 2(a) together with the magnetic moments of the Co adatom and of the Pt surface atoms, as well as the direction of the magnetization easy axis. The Co adatom lies at 1.59 Å from the Pt surface with a Co-Pt bond length of 2.34 Å, 17% shorter than the bulk Pt-Pt value. The calculated magnetic moment of the Co adatom is $2.03\mu_B$, in good agreement with the experimental value of $2.1\mu_B$ obtained from x-ray magnetic circular dichroism (XMCD) spectroscopy,[10] and with previous theoretical results based on the force theorem and on the same local-density approximation (LDA) functional[14] (Table I). Adsorption on the hcp is 0.1 eV higher in energy than on the fcc, and the equilibrium local environment and magnetic moments for the two sites are very similar with the difference in calculated quantities being always smaller than 2%. The Co adatom induces a magnetization of the Pt surface so that the Pt atoms nearest neighbors to the Co adatom have a

TABLE I. Co adatom supported by the Pt(111) surface. Magnetic moments of the Co atoms and of their nearest-neighbor Pt atoms. Magnetic anisotropy energy (MAE, in meV) and direction of the easy axis expressed in terms of the angles θ and ϕ defined in Fig. 3.

	Exp.	DFT-LDA		
	Ref. 10	This work		Ref. 14
		Relaxed	Unrelaxed	Unrelaxed
μ(Co)(μ_B)	2.1	2.03	2.18	2.21
μ(Pt)(μ_B)		0.20	0.11	
MAE (meV)	9.0	4.8	9.2	5.9
(θ, ϕ)	(0.0,0.0)	(0.0,0.0)	(0.0,0.0)	(0.0,0.0)

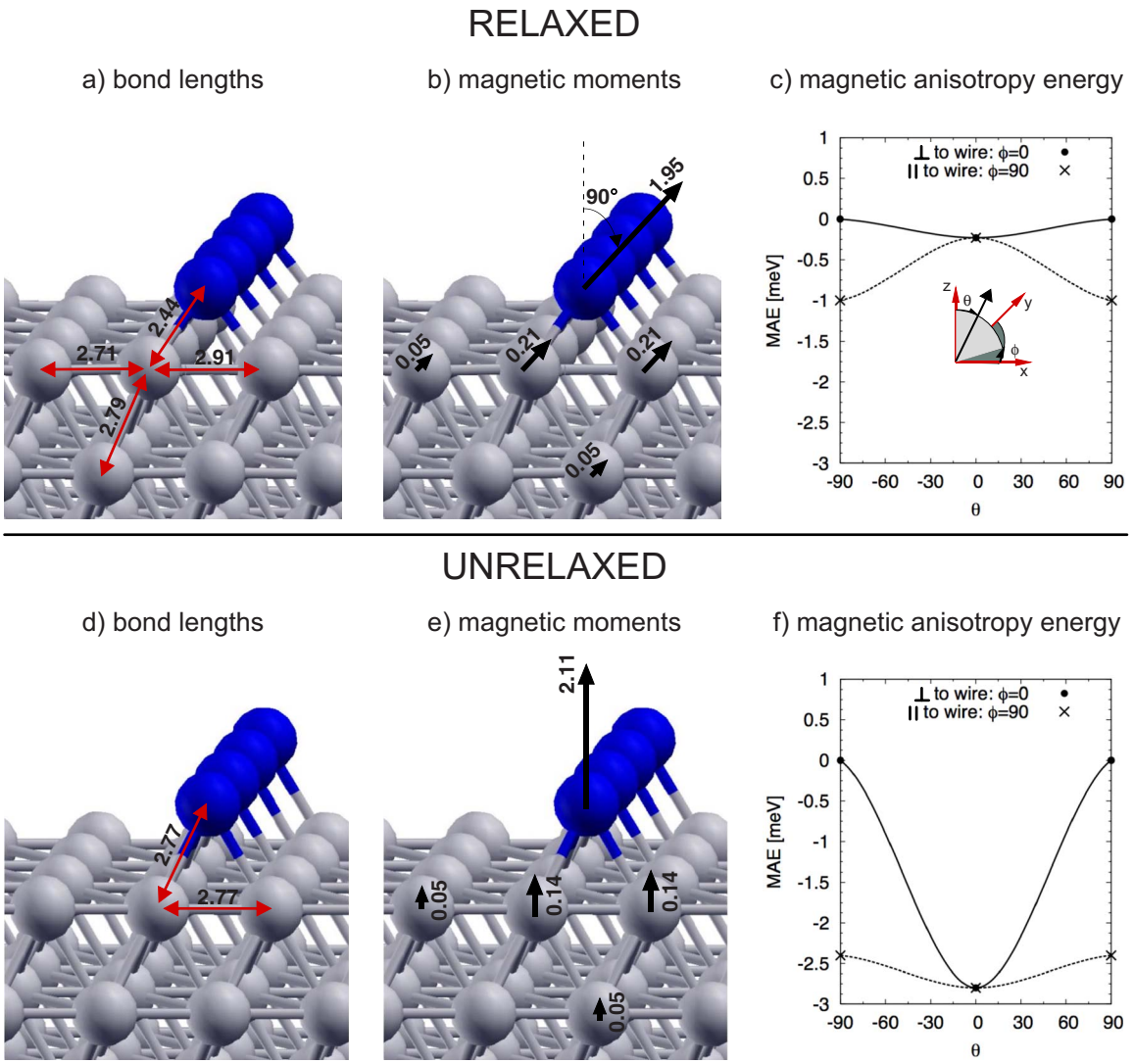

FIG. 3. (Color online) Relaxed (top) and unrelaxed (bottom) configurations of a Co nanowire supported by a Pt (111) surface. Panels (a) and (d): Co-Pt bond lengths expressed in Å. Panels (b) and (e): Magnetic moments directed along the easy-magnetization axis in units of μ_B. [Note in panel (b) the arrow is oriented parallel to the wire.] Panels (c) and (f): Total energy as a function of the Co magnetic-moment direction expressed in terms of the angles θ and ϕ defined in the inset. Atoms are represented as described in Fig. 1.

magnetic moment of $0.20\mu_B$. The Pt magnetization rapidly decreases with the Pt-Co distance so that the magnetic moment of all the other Pt atoms is lower than $0.06\mu_B$.

The easy-magnetization axis is predicted to be orthogonal to the Pt surface, in agreement with experimental observations,[10] while the calculated MAE of 4.8 meV is underestimated with respect to the experimental value (Table I). We notice the agreement between the experiment and the MAE is fortuitously better (9.2 meV) when employing unrelaxed geometry [see Fig. 2(b)]. This extreme sensitivity of the local magnetic structure on the details of the atomic coordination poses rather severe limits to the predictive power of DFT calculations. However it also points to the opportunities offered to nanoscale materials engineering for tailoring the properties of magnetic devices. This will be further discussed in the cases of the Co wires supported by Pt surfaces where the effect is more dramatic, affecting not only the value of the MAE but also the direction of the easy axis.

B. Co nanowires on Pt surfaces

1. Co nanowires on the flat Pt(111) surface

We now analyze the properties of Co nanowires supported by a flat Pt(111) surface. Even though it is not possible to stabilize Co nanowires on flat Pt(111) surfaces (adatoms would tend to aggregate forming clusters and islands), we nevertheless consider this case since its analysis allows us to separate out the effects of the step from those of the surface in the magnetic properties of the Co wires.

The results for the structural and magnetic properties of Co nanowires on Pt(111) surfaces are summarized in Fig. 3 and Table II. The top panels of Fig. 3 display the equilibrium geometry [Fig. 3(a)], the direction of the easy axis of magnetization together with the magnetic moments [Fig. 3(b)], and the total energy as a function of the magnetic moment direction [Fig. 3(c)].

TABLE II. Co wire supported by the Pt(111) surface. Magnetic moments of the Co atoms and of their nearest-neighbor Pt atoms (Pt_{NN}). MAE (in meV) and direction of the easy axis, expressed in terms of the angles θ and ϕ defined in the inset of Fig. 3.

	DFT-LDA		
	This work		Ref. 14
	Relaxed	Unrelaxed	Unrelaxed
$\mu(\mathrm{Co})(\mu_B)$	1.95	2.12	2.11
$\mu(\mathrm{Pt}_{NN})(\mu_B)$	0.21	0.14	
MAE	2.8	1.0	3.3
(θ,ϕ)	(0.0,90.0)	(0.0,0.0)	(0.0,0.0)

The Co wire is predicted to be at 1.74 Å from the Pt surface, resulting in Co-Pt bond length of 2.44 Å. Co wires on Pt(111) induce a surface strain: The Pt-Pt bond length below the Co wire increases by 5% upon wire formation from 2.77 (in-plane surface lattice constant) to 2.91 Å. Of course, we expect that the observed strain will be proportional to the surface stress determined by the Co overlayer, which in turn will depend on coverage. The present simulation utilizes a geometry characterized by periodically repeated wires. It is to be expected that, for an isolated wire, the stress will be inhomogeneous and will vanish far from the wire.

The calculated magnetic moment of the wire in the equilibrium configuration is $1.95\mu_B$ per Co atom (Table II), smaller than the corresponding value obtained for the Co adatom. Similarly to the adatom case, the Co wire induces a magnetic moment of $0.14\mu_B$ on the neighboring Pt surface atoms.

The easy axis of magnetization for the equilibrium geometry is predicted to be parallel to the wire [Fig. 3(b)] with a MAE of just 1 meV (Table II). The total energy, as a function of the direction of the magnetic moment defined by the angles (θ,ϕ) [Fig. 3(c)], displays a double-well structure for angular variations of the magnetic moment in both planes parallel ($\phi=90°$) and perpendicular ($\phi=0°$) to the wire.

The only available DFT theoretical results for these structures are based on the linear muffin-tin orbital (LMTO) method and are performed for the unrelaxed geometry only.[14] In order to compare the predictions of our method with previous data, we consider now, besides the fully relaxed structures, also the same unrelaxed geometry defined in that previous work. This geometry and the corresponding results are displayed in the bottom panels of Fig. 3. The calculated magnetic moment is now $2.12\mu_B$, in good agreement with the previously reported value of $2.11\mu_B$,[14] and is larger than the corresponding value obtained for the fully relaxed geometry (Table II). The smaller value of the atomic magnetic moment in a Co wire then, for an isolated adatom, is consistent with the expectation that the moment decreases with increasingly atomic coordination. The higher value of the moment predicted for the unrelaxed geometries, which are characterized by a larger Co-Pt bond length, is also consistent with the increase in the "effective coordination" by decreasing the bond length. Similarly, the MAE is predicted to be 2.8 meV, larger than that calculated for the equilibrium geometry, and in good agreement with the value previously calculated with the force theorem (3.3 meV).[14]

It is the direction of the easy-magnetization axis that displays the most remarkable variation with respect to the local adsorption geometry of the surface-supported Co wire. In this case, the easy axis is predicted to be perpendicular to the wire and to the surface, in agreement with the previous studies, but being rotated by 90° with respect to the one obtained by relaxing the surface structure. Also in this unrelaxed geometry, the total energy as a function of the direction of the magnetic moment displays a double-welled structure [Fig. 3(f)] but here the minimum for variations of the angular momentum in both the parallel and perpendicular is obtained for $\phi=0°$ and $\theta=0°$ (see also Table II).

2. Co nanowires on a vicinal Pt(442) surface

We now consider the effect of surface steps on the magnetic properties of supported Co wires by studying the case of a vicinal Pt(442) surface, whose steps are decorated by Co nanowires. The equilibrium structure is displayed in Fig. 4(a). In this configuration, each Co atom has five Pt nearest neighbors. The interaction of the step atoms with a supported Co wire has the effect of smoothening the step. These results are derived from the strong contraction of the Co-Pt_{II} bond length (2.43 Å) with respect to a clean Pt(442) surface and from the elongation of the Pt_{III}-Pt_{IV} bond length (2.98 Å).

Figure 4(b) displays the magnetic moments of the Co and Pt atoms, and the direction of the easy axis for the wire in the relaxed configuration. The calculated magnetic moment is $2.00\mu_B$ per Co atom (Table III), in between the values obtained for the Co adatom and for the Co wire on the Pt(111) surface. The magnetic moment induced on the Pt atoms, nearest neighbors to the Co wire, range between $0.18\mu_B$ and $0.24\mu_B$. As reported in Table III, these results are consistent with the experimental values ($2.1\mu_B$) measured with XMCD (Ref. 18) for monoatomic Co nanowires assembled on a vicinal Pt(997) surface. Moreover, our results are in very good agreement with those calculated with the force field methods, and with the corrected generalized gradient approximation (GGA) for the exchange and correlation potential. The latter calculations report $2.11\mu_B$ and $0.24\mu_B$ (Ref. 12) for the magnetic moments of the Co and its nearest-neighbor Pt atoms, correspondingly (Table III). Beyond the first coordination shell, the induced Pt magnetization decreases very rapidly with the distance from the Co atoms, as displayed in Fig. 4(b). The magnetic moment of the Pt atoms second-nearest neighbors to the Co atom has already decreased to $0.05\mu_B$. The intermediate value of the magnetic moment predicted for the wire of the step, as compared to those predicted on the clean surface and for an adatom, seems to contradict the trend of the moment with respect to the local coordination. It is possible that this intermediate value results from the combined effect of an increased coordination of the Co atoms and of a decreased coordination of the neighboring Pt atoms, whose local moments are indeed predicted to be located at the step edge of the terraces, which display a sizable magnetization

The total energy as a function of the direction of the magnetic moment is displayed in Fig. 4(c). The low symmetry of

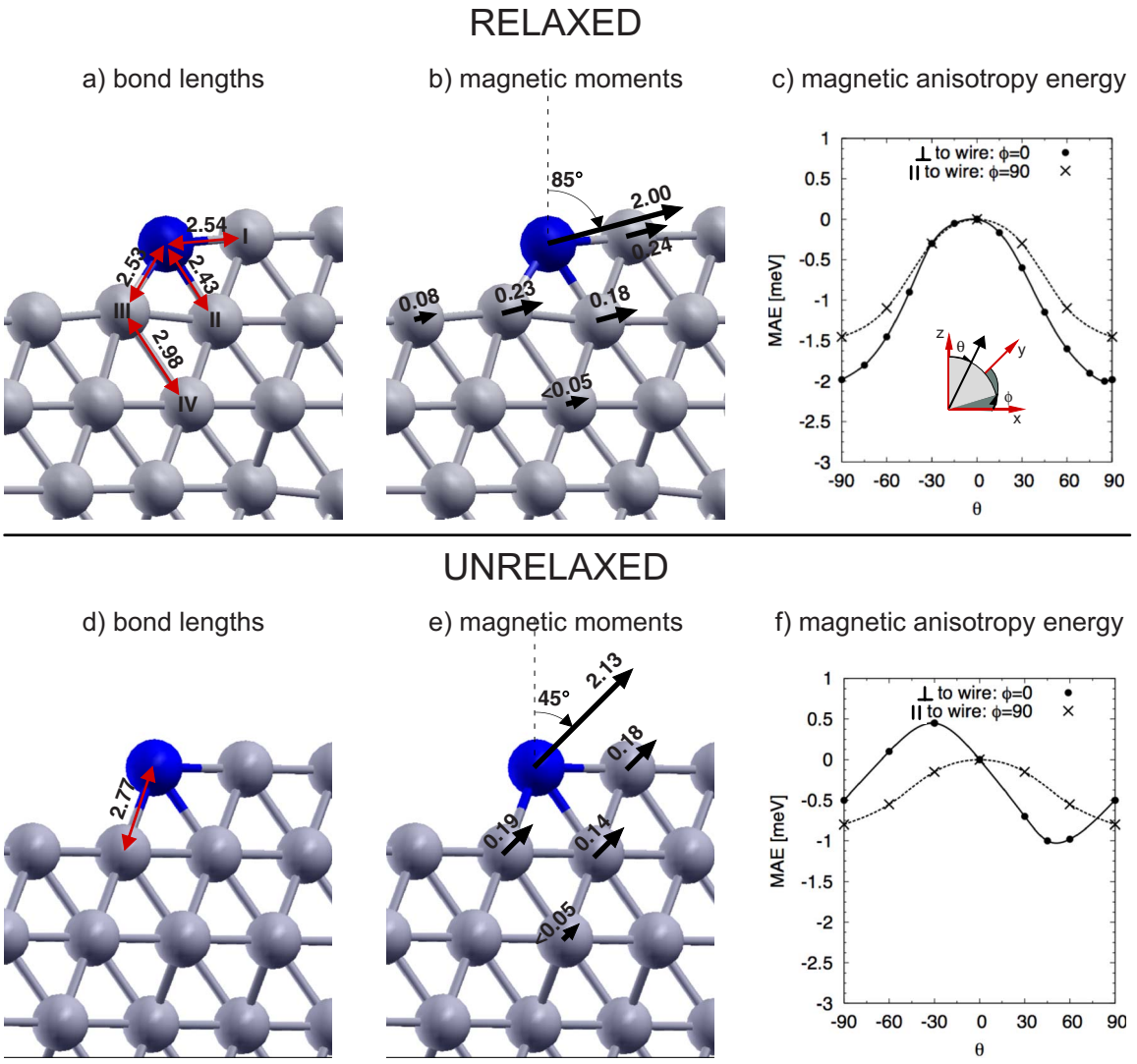

FIG. 4. (Color online) Relaxed (top) and unrelaxed (bottom) configurations of a Co nanowire supported by a Pt (442) surface. Panels (a) and (d): Co-Pt bond lengths expressed in angstrom. Panels (b) and (e): Magnetic moments directed along the easy-magnetization axis in units of μ_B. Panels (c) and (f): Total energy as a function of the Co magnetic-moment direction expressed in terms of the angles θ and ϕ defined in the inset. Atoms are represented as described in Fig. 1.

the step sites is reflected into the magnetic anisotropy energy, which, differently from the cases previously analyzed, is not symmetric with respect to variations of the magnetic-moment direction away from the surface normal (θ=0). The calculated value of the MAE for the relaxed geometry (2.0 meV) is in excellent agreement with experiment, reporting 2.0 ± 0.2 meV per Co atom.[18] The direction of the easy axis for the stepped surface is predicted to be orthogonal to the wire (ϕ=90°), forming an angle of θ=85° with respect to the normal of the (111) terrace [see Table III, and Figs. 4(b) and

TABLE III. Co nanowire supported by the Pt(442) surface. Magnetic moments of the Co atoms and of their nearest-neighbor Pt atoms (Pt_{NN}). MAE (in meV) and direction of the easy axis, expressed in terms of the angles θ and ϕ defined in Fig. 3.

	Exp	DFT-LDA		DFT-PBE	
	Ref. 18	This work		Ref. 12	
		Relaxed	Unrelaxed	Relaxed	Unrelaxed
μ(Co)(μ_B)	2.1	2.00	2.13	2.11	2.14
μ(Pt_{NN})(μ_B)		0.23	0.19	0.24	0.17
MAE (meV)	2.0	2.0	1.5	2.2	2.5
(θ, ϕ)	(43,0)	(85,0)	(45,0)	(85,0)	(45,0)

4(c)]. It is interesting to compare the direction of the easy axis for this case, which is orthogonal to the wire and almost coplanar to the surface, with the easy axis direction calculated for the Co wire on the Pt(111) terrace, predicted to be parallel to the wire. This comparison indicates that the presence of the step, induces a rotation of the easy axis by 90°.

The predicted direction of the easy axis, (ϕ=90° and θ =85°) is in agreement with the prediction by Baud *et al.*,[12] reporting exactly the same value. Notice that both theoretical work predictions are off by ≈40° from the experimental value. The hysteresis loops[18] measured in the superparamagnetic and in the ferromagnetic regimes for this system show that the easy-magnetization axis lays in the plane perpendicular to the wire (ϕ=90°), and its direction forms an angle θ of 43° with respect to the axis perpendicular to the (111) terrace plane. The reasons for this discrepancy are not clear but the analysis of the unrelaxed geometry (bottom panels of Fig. 4) provides some insight.

The direction of the easy axis calculated for the unrelaxed structure is θ=45° [Figs. 4(e) and 4(f)] and is in much better agreement with experimental findings. This agreement is fortuitous since the unrelaxed structure is to some extent arbitrary. This result shows that differences in the local structure of ≈10% (Co-Pt and Pt-Pt bond lengths differ by ≈0.2 Å between the relaxed and unrelaxed geometries) have the effect of rotating the easy axis of the nanowire by more than 40°. The same strong dependence of the easy axis direction is reported for a different terrace length and obtained with a different functional,[12] and can therefore be expected to be a rather general feature.

Size effects might in principle play an important role into the magnetic properties of supported magnetic nanowires. Indeed theoretical analysis on finite Co chains supported by a stepped Cu surface[34] shows that edge effects on structural and magnetic properties are mostly concentrated in the last two to four terminating atoms of the wire, and are thus relevant only for very short chains. We notice that the average length of the Co wires supported by the vicinal Pt surfaces measured experimentally is ≈80 atom.[18] The infinite wires considered in our study are therefore a good model for the atoms comprising the central part of these rather long magnetic wires.

IV. CONCLUSIONS

The electronic, structural, and magnetic properties of Co-based nanostructures supported by flat and stepped Pt surfaces have been studied with periodic noncollinear DFT calculations that include the spin-orbit coupling into fully relativistic pseudopotentials. The calculated MAE, magnetic moments, and easy axis direction have been shown to be very sensitive on the local atomic environment around the Co nanostructures. We show that atomic displacements of 0.1–0.2 Å can modify both the MAE by 48% and the direction of the easy axis by as much as 90°.

We notice that in some studied cases, the MAE calculated for a bulklike terminated surface are in remarkably good agreement with the experimental results but this agreement has to be considered as fortuitous to some extent. In the case of the adatom, for example, the theoretical value of the MAE calculated for the unrelaxed structure is in perfect agreement with the experiments. A similar good agreement is obtained for the direction of the easy axis in the case of the unrelaxed Co nanowire on the stepped Pt surface. In both cases, geometry optimization makes the theoretical predictions depart from the corresponding experimental values. This seems to suggest that either the atomic relaxation or its effect on the magnetic structure is overestimated.

This extreme sensitivity of the magnetic properties on the local atomic environment of magnetic nanostructures represents an obstacle for theoretical predictions since the present energy functionals are probably not accurate enough to yield the relaxed atomic coordinates with the necessary precision. The energy differences due to the anisotropic effects are in any case very small and stretch the predictive power of state-of-the-art DFT calculations to their limits.

If this sensitivity certainly limits the predictive power of available theoretical and simulation methods, it also offers great opportunities for tailoring the properties of magnetic devices by engineering the materials at the nanoscale. Also, this sensitivity suggests that a proper account of lattice vibrations—which determine thermal fluctuations of the bond lengths—would probably affect significantly the predicted magnetic properties.

ACKNOWLEDGMENTS

We wish to thank Andrea Dal Corso for fruitful discussions and for providing help with the relativistic pseudopotential method. Calculations have been made possible by the SISSA-CINECA scientific agreement and by the allocation of computer resources from INFM-CNR Progetto Calcolo Parallelo. Graphics have been generated with the XCRYSDEN molecular program (Ref. 35).

*Present address: Università di Tor Vergata, via della Ricerca Scientifica 1, 00134 Roma, Italy.

[1] G. Christou, D. Gatteschi, B. Hendrickson, and R. Sessoli, MRS Bull. **25**, 66 (2000).

[2] N. M. Leuenberger and D. Loss, Nature (London) **410**, 789 (2001).

[3] T.-J. Yoon, W. Lee, Y.-S. Oh, and J.-K. Lee, New J. Chem. **27**, 227 (2003).

[4] R. N. Grass, E. K. Athanassiou, and W. J. Stark, Angew. Chem., Int. Ed. **46**, 4909 (2007).

[5] R. P. Cowburn, D. K. Koltsov, A. O. Adeyeye, M. E. Welland, and D. M. Tricker, Phys. Rev. Lett. **83**, 1042 (1999).

[6] A. M. Gomes, M. A. Novak, R. Sessoli, A. Caneschi, and D. Gatteschi, Phys. Rev. B **57**, 5021 (1998).

[7] A. B. Klautau and S. Frota-Pessôa, Phys. Rev. B **70**, 193407 (2004).
[8] Ž. Šljivančanin, Z. S. Popović, F. R. Vukajlović, and A. Baldereschi, Phys. Rev. B **74**, 134412 (2006).
[9] R. Wood, IEEE Trans. Magn. **36**, 36 (2000).
[10] P. Gambardella, S. Rusponi, M. Veronese, S. Dhesi, C. Grazioli, A. Dallmeyer, I. Cabria, R. Zeller, P. H. Dederichs, K. Kern, C. Carbone, and H. Brune, Science **300**, 1130 (2003).
[11] P. Wahl, P. Simon, L. Diekhöner, V. S. Stepanyuk, P. Bruno, M. A. Schneider, and K. Kern, Phys. Rev. Lett. **98**, 056601 (2007).
[12] S. Baud, Ch. Ramseyer, G. Bihlmayer, and S. Blügel, Phys. Rev. B **73**, 104427 (2006).
[13] S. Baud, Ch. Ramseyer, G. Bihlmayer, and S. Blügel, Surf. Sci. **600**, 4301 (2006).
[14] B. Lazarovits, L. Szunyogh, and P. Weinberger, Phys. Rev. B **67**, 024415 (2003).
[15] A. Gelfert and W. Nolting, J. Phys.: Condens. Matter **13**, R505 (2001).
[16] N. D. Mermin and H. Wagner, Phys. Rev. Lett. **17**, 1133 (1966).
[17] P. Gambardella, M. Blank, L. Bürgi, K. Kuhnnke, and K. Kern, Surf. Sci. **449**, 93 (2000).
[18] P. Gambardella, A. Dallmeyer, K. Maiti, M. C. Malagoli, W. Eberhardt, K. Kern, and C. Carbone, Nature (London) **416**, 301 (2002).
[19] J. Korringa, Physica (Amsterdam) **13**, 392 (1947).
[20] W. Kohn and N. Rostoker, Phys. Rev. **94**, 1111 (1954).
[21] O. K. Andersen, Phys. Rev. B **12**, 3060 (1975).
[22] D. Vanderbilt, Phys. Rev. B **41**, 7892 (1990).
[23] A. Dal Corso and A. Mosca Conte, Phys. Rev. B **71**, 115106 (2005).
[24] A. Smogunov, A. Dal Corso, A. Delin, R. Whet, and E. Tosatti, Nat. Nanotechnol. **3**, 22 (2008).
[25] M. Weinert, R. E. Watson, and J. W. Davenport, Phys. Rev. B **32**, 2115 (1985).
[26] A. Mosca Conte, Ph.D. thesis, SISSA, 2007.
[27] T. Oda, A. Pasquarello, and R. Car, Phys. Rev. Lett. **80**, 3622 (1998).
[28] R. Gebauer, S. Serra, G. L. Chiarotti, S. Scandolo, S. Baroni, and E. Tosatti, Phys. Rev. B **61**, 6145 (2000).
[29] S. H. Vosko, L. Wilk, and M. Nusair, Can. J. Phys. **58**, 1200 (1980).
[30] S. Baroni, A. Dal Corso, S. de Gironcoli, and P. Giannozzi (http://www.pwscf.org/); See also (http://www.quantum-espresso.org)
[31] Fully relativistic USPPs for the elements studied in this work are available in the Quantum Espresso pseudopotential library (http://www.pwscf.org/pseudo.htm).
[32] H. J. Monkhorst and J. D. Pack, Phys. Rev. B **13**, 5188 (1976).
[33] M. Methfessel and A. T. Paxton, Phys. Rev. B **40**, 3616 (1989).
[34] Š. Pick, P. A. Ignatiev, A. L. Klavsyuk, W. Hergert, V. S. Stepaniuk, and P. Bruno, J. Phys.: Condens. Matter **19**, 446001 (2007).
[35] A. Kokalj, J. Mol. Graphics Modell. **17**, 176 (1999); Code available from (http://www.xcrysden.org/).